O (^{3}P) + C_2H_2/C_2H_4/·CH_3 REACTIONS UNDER KINETIC CONTROL IN ^{4}HE NANODROPLETS

by

BRADLEY WILLIAM ACREY

(Under the Direction of Gary E. Douberly)

ABSTRACT

The reactions between small hydrocarbons within oxidative environments are at the forefront of present day research. A review of Helium Nanodroplet Isolation (HENDI) spectroscopy is given to highlight the advantages of this well-developed technique compared to similar gas phase experiments. The details for a high temperature pyrolysis source, capable of producing a beam of O (^{3}P) atoms, will be shown that can be implemented with the HENDI technique. A sequential pick-up technique to study the reactions of O (^{3}P) + C_2H_2/C_2H_4/·CH_3 is described, which can effectively "dope" the reactants within the droplet. We will look to gain insight into the chemical energetics of these prototype reactions with atomic oxygen. These proposed reactions can be carried out in the low temperature, dissipative environment of helium nanodroplets. This technique affords us the capability to study these reactions with effectively zero background due to the weakly perturbing He solvent. High resolution ro-vibrational spectroscopy of these reactions is still lacking in both the gas phase and matrix isolation. Our goal is to unravel the spectroscopy of the three proposed reactions in the CH stretching region of the IR spectrum (2800-3300 cm^{-1}). Quantum chemical computation methods will be used for structural assignments and comparison with our experimental spectra.

INDEX WORDS: HENDI, helium nanodroplets, O (^{3}P), ro-vibrational spectroscopy, IR spectra, matrix isolation, and gas-phase.

$O\ (^3P) + C_2H_2/C_2H_4/\cdot CH_3$ REACTIONS UNDER KINETIC CONTROL IN ^4HE NANODROPLETS

by

BRADLEY WILLIAM ACREY

B.S., University of Georgia, 2011

A Thesis Submitted to the Graduate Faculty of The University of Georgia in Partial Fulfillment of the Requirements for the Degree

MASTER OF SCIENCE

ATHENS, GEORGIA

2014

© 2014

Bradley William Acrey

All Rights Reserved

$O\ (^3P) + C_2H_2/C_2H_4/\cdot CH_3$ REACTIONS UNDER KINETIC CONTROL IN ^4HE NANODROPLETS

by

BRADLEY WILLIAM ACREY

Major Professor: Gary E. Douberly

Committee: Michael A. Duncan
Geoffrey D. Smith

Electronic Version Approved:

Dr. Julie Coffield
Interim Dean of the Graduate School
The University of Georgia
December 2014

ACKNOWLEDGEMENTS

I would like to thank my major professor, Gary Douberly, for allowing me the opportunity to work with him over the last three plus years. I have gained knowledge in physical chemistry and more specifically in spectroscopy under Gary's tutelage. I am grateful for the many discussions during group meetings and office visits back and forth down the hall whenever I would have questions or concerns. I would also like to thank my group members, past and present; Alex Morrison, Steven Flynn, Tao Liang, Chris Moradi, Caitlyne Shirley, Emmanuel Obi, and Joseph Brice, for their assistance and meaningful discussion. I can't neglect mentioning two phenomenal post docs, Dr. Paul Raston and Dr. Christopher Leavitt, who were of great help during my time here at UGA.

TABLE OF CONTENTS

Page

LIST OF FIGURES

Page

CHAPTER 1

HELIUM NANODROPLET ISOLATION

1.1 Background

The liquidification of helium was achieved by Onnes in 1908, and set up the century for more detailed work on this fascinating solvent.[1] A series of experiments performed from 1937-1938 led to the discovery of the superfluid properties of liquid helium.[2] It was observed that the viscosity of ^{4}He decreased to almost zero when it was cooled below the λ-point around 2.17 K. Theoretical work by Landau[3] from the 1940's, provided a two-fluid model describing how helium consists of a superfluid and normal fluid fraction. This model was confirmed by the famous Andronikashvilli experiment in 1946 which featured a large bath of helium containing a series of rotating discs within the bath. As the temperature of the helium was decreased, the liquid helium experienced less friction, until zero viscosity was observed.[4] In the first spectroscopic experiment with helium, Goyal et al.[5] used a line tunable, CO_2 laser to excite the ν_3 band in SF_6. They compared the differences between infrared spectra of SF_6 in helium to spectra from other rare gas matrices and noticed that the spectrum obtained in helium had much better resolution. As laser technology advanced, the first rotationally resolved spectrum of SF_6 in helium nanodroplets was obtained using a diode laser in 1994.[6] This experiment also confirmed theoretical models of the solvation characteristics of the droplet. The SF_6 molecule was found to be solvated within the droplet and the *B* rotational constant was a factor of 3 smaller than the corresponding gas phase value. The explanation of this

reduced value was said to be caused by adiabatic following of 8 helium atoms; the He atoms rotate with the molecule and cause an increase in the effective moment of inertia.[7] The vibrational frequency was not shifted much compared to the gas-phase value, whereas large matrix shifts are typically observed in rare gas matrices. The overall symmetry of SF_6 was the same as the gas-phase and by using a slightly modified set of rotational constants, the rotational spectrum could be simulated and interpreted. This paved the way for the field of helium nanodroplet isolation spectroscopy, HENDI, as it would later become known, to blossom into a vital tool for spectroscopic analysis. Brink and Stringari predicted the temperature of the droplet to be 0.32 K in 1990. Their calculations were based on the properties of bulk ^{3}He and ^{4}He and employed the liquid-drop model.[8] An experimental determination of the rotational temperature was obtained for the OCS molecule embedded in helium droplets in the work of Frochtenicht et al. The 0.37 K temperature is consistent with the theoretical value predicted by Stringari. The superfluid properties of the droplet play an important role in allowing embedded molecules to rotate with sufficiently long coherence times to display well-resolved rotational structure due to the presence of a "phonon gap" that extends up to approximately 5 cm^{-1}, which places the low-lying rotational states of a molecule (namely, those populated at 0.37 K) in a region where the density of bulk phonons are low. The weak coupling between the molecular rotation and the bulk phonons of ^{4}He gives rise to the long rotational lifetimes that enable us to perform high-resolution matrix isolation spectroscopy. ^{3}He has no phonon gap and stronger coupling between the molecular rotation and bulk phonons that leads to shorter rotational lifetimes. Liquid helium is optically transparent below 161,000 cm^{-1}, allowing for spectroscopic

measurements with zero background. Spectroscopic measurements have been made with infrared (IR) radiation, following the capture of atoms or molecules within the droplet. Helium nanodroplets have proven effective at these low temperatures in delivering a technique with limited matrix broadening that also allow for the study of reactions and the formation of new complexes by using a sequential pick-up technique. At present all molecular spectra in liquid helium have been obtained in helium droplets produced in free jet expansions, mostly of gaseous He but also in a few cases in expansions of the liquid.[9] Chapter 2 of this thesis will go into more detail regarding the experimental methodology of helium nanodroplet isolation.

1.2 Recent Work

The field of helium nanodroplet spectroscopy has seen an emergence of new experiments in the past decade. The IR spectroscopy of methyl[10], ethyl[11], vinyl[12], hydroxyl[13], and propargyl[14] radicals; HO_3[15] and $HO_3(O_2)_n$[16]; several alkyl + O_2 reactions[16-19], and Al—$(CO)_n$[20] and Al + HCN[21]. In Chapter 3, we propose the design of a new source capable of producing oxygen atoms. This source will enable the study of reactions, such as O + C_2H_2/C_2H_4/·CH_3, and potentially other O + R radicals, which may lead to the formation of highly reactive complexes in situ. Combustion reaction byproducts have seen an increase in spectroscopic significance in recent years due to the overwhelming environmental issues regarding the use of fossil fuels. Some reactions are being reinvestigated using higher resolution techniques that are now available, while others lack any clear spectroscopic assignment. This is the case for alkyl + oxygen atom complexes. The focus of Chapter 4 will be on a few prototype reactions that may be targets.

References

1. Onnes, H. K. Commun. Phys. Lab. Univ. Leiden 1908, 108, 3.
2. Kapitsa, P. *Nature* 1938, **141**,74-75.
3. Landau, L. D. J.Phys. *USSR* 1941, **5**, 71.
4. Andronikashvilli, E. *Journal of Physics* 1946, 3, 201-206.
5. Goyal, S.; Schutt, D. L.; Scoles, G. *Phys. Rev. Lett.* 1992, 69, 933-936.
6. Frochtenicht, R.; Toennies, J. P.; Vilesov, A. *Chem. Phys. Lett*. 1994, 229, 1-7.
7. Hartmann, M.; Portner, N.; Sartakov, B.; Toennies, J. P.; Vilesov, A. F. *J. Chem. Phys.* 1999, 110, 5109-5123.
8. Brink, D. M.; Stringari, S. Zeitschrift Fur Physik D-Atoms Molecules and Clusters **1990**, 15, 257.
9. Toennies, J. P.; Vilesov, A. F. *Angew. Chem., Int. Ed*. **2004**, 43, 2622−2648.
10. Morrison, A. M.; Raston, P. L.; Douberly, G. E. *J. Phys. Chem. A* **2012**, DOI: 10.1021/jp310083j.
11. Raston, P. L.; Agarwal, J.; Turney, J. M.; Schaefer, H. F.; Douberly, G E. *J. Chem. Phys.* **138**, 194303 (2013).
12. Raston, P. L.; Liang, T.; Douberly, G. E. *J. Chem. Phys*. **2013**, 138.
13. Raston, P. L.; Liang, T. ; Douberly, G. E. *J. Phys. Chem. A* **2013**, 117.
14. Küpper, J.; Merritt, J. M.; Miller, R. E. *J. Chem. Phys*. **2002** 647-652, 117.
15. Raston, P. L.; Liang, T. ; Douberly, G. E. *J. Chem. Phys*. **2012**, 137, 184302.
16. Liang, T.; Raston, P. L. ; Douberly, G. E. *Chem. Phys. Chem*. **2012**, DOI: 10.1002/cphc.201200712.
17. Morrison, A. M. ; Agarwal, J. ; Schaefer, H. F. ; Douberly, G. E. *J. Phys. Chem.*

A **2012**,116, 5299 - 5304.

18. Moradi, C. P. ; Morrison, A. M. ; Klippenstein, S. J. ; C. Goldsmith, F. ; Douberly, G. E. *J. Phys. Chem. A* **2013**, 117, 13626-13635.

19. Leavitt, C. M. ; Moradi, C. P. ; Acrey, B. W. ; Douberly, G. E. *J. Chem. Phys*. **2013**, 139, 234301.

20. Liang, T. ; Flynn, S. D. ; Morrison, A. M. ; Douberly, G. E. *J. Phys. Chem. A* **2011**, 115, 7437 - 7447.

21. Liang, T.; Douberly, G. E. *Chem. Phys. Lett*. **2012**, 551, 54 - 59.

CHAPTER 2

EXPERIMENTAL METHOD

2.1 Droplet Formation

Helium nanodroplets are made by free jet expansion of ultra-high purity helium gas from a high pressure, cold, continuous wave (cw) nozzle. The process of free jet expansion of high pressure helium was done first by Becker in 1961.[1] Helium at 20–90 bar backing pressure is expanded through an approximately 5 micron diameter nozzle, cooled to low temperature (8–28 K). A skimmer is used following this expansion to form a well-collimated beam, which subsequently traverses one or more pick-up cells (PUCs). The size of the nozzle aperture is largely determined by the pumping speed of the source pump. Droplets can be made in various sizes by changing the temperature or backing pressure, typical operation conditions involve the use of 99.9995% pure helium (30 bar) backing pressure with the nozzle temperature set at 17 K, which results in the formation of droplets with an average size of ~5000 helium atoms.[2, 3] The size of the droplets follow a log-normal statistical distribution (In the equation shown below) that was formulated by work done by Knuth, Schilling, and Toennies.[3]

$$P_N(N) = \left(N\sigma\sqrt{2\pi}\right)^{-1} \exp\left[-\frac{(ln\, N - \mu)^2}{2\sigma^2}\right]$$

Their work led to empirically established scaling laws that can be used to calculate mean droplet size as a function of temperature. For example, a nozzle temperature of 15 K would generate droplets having approximately 10,000 helium atoms on average.

Spectroscopic studies benefit with smaller droplets because fewer droplets tend to form when the mean size of the droplets is large. The lower number of droplets present leads to weaker spectroscopic signals because less dopant molecules are being detected and averaged. As you decrease the temperature of the nozzle, larger droplets are formed. The ability to vary the droplet size as a function of temperature remains critical given that the helium atoms are capable to dissipate 5 cm^{-1} of energy per atom. This is especially important for reactions where energy is released in the formation and breaking of bonds. In the case of the allyl + O_2 addition reaction ($\Delta H \approx$ -18 kcal/mol or -6000 cm^{-1}), the evaporation of ~1250 helium atoms was necessary.[4] The droplets must be large enough to keep the molecules solvated within the droplet prior to irradiation with an IR laser (~3000 cm^{-1}), which ultimately leads to the further evaporation of ~600 helium atoms.

2.2 Doping the Droplets

We use a well-developed pick-up technique to effectively add our dopants into the droplets.[5] Dopants (atoms or molecules) are introduced into the spectrometer in a variety of ways. The majority of experiments performed utilize a high temperature (up to ~1800 K) pyrolysis source.[6, 7] This effusive pyrolysis source is pictured below in Fig. 1, and features water cooled copper electrodes with a quartz tube at the tip. A tantalum filament is wrapped loosely around the quartz tube and a current is applied to resistively heat the tube and achieve pyrolysis of precursor molecules to yield the desired dopant. This source is load-lockable with the capability of rough pumping away contamination prior to entering the vacuum chamber.[5] The sample is held in a suitable container and is shown pictorially on the far left in Fig. 2.1.

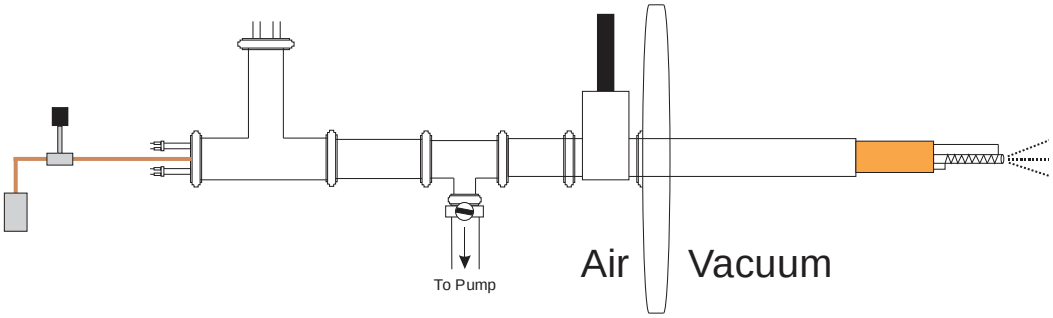

Fig. 2.1. Pyrolysis source for use with HENDI spectrometer.

In the case of the production of allyl radical, 3-butenyl nitrite ($H_2C=CHCH_2CH_2ONO$) was used as the precursor, and upon high temperature pyrolysis fragmented into allyl, formaldehyde, and nitric oxide (NO). The PUC pressure and pickup process follow a Poisson distribution and have been described elsewhere.[8, 9] For droplets in the size range of 1000-5000 atoms, and a pick-up cell length of 10 cm, a pressure of 10^{-6} Torr will permit the pick-up of only one molecule or atom per droplet using this statistical approach.[5] Molecular oxygen was added via a static, differentially pumped PUC where a constant pressure of 2.0 x 10^{-6} Torr was maintained by using a fine metering valve to assure that a single O_2 molecule was picked up in the droplet.

2.3 Experimental diagram

The HENDI spectrometer is shown below in Fig. 2.2. Chamber 1 (left) features the droplet source and skimmer, Chamber 2 (center) features three in-line PUC's, and Chamber 3 (right) feature the quadrupole mass spectrometer with 90° bender and the Channeltron® electron multiplier tube at the top. The droplet beam is illustrated in blue to show the path it travels through the instrument.

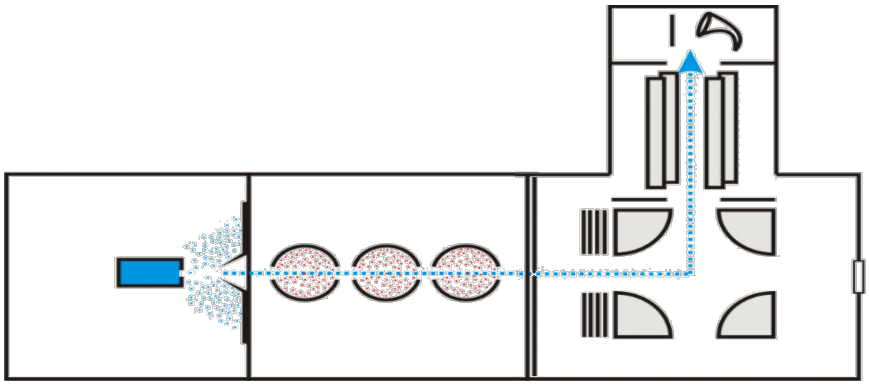

Fig. 2.2. Experimental diagram of HENDI spectrometer.

Differential pumping is required to keep the chambers at high vacuum (10^{-6} - 10^{-7} Torr) for the PUC chamber using diffusion pumps backed by small mechanical pumps. The mass spec chamber is kept at lower vacuum to eliminate the possibility of contaminant species coming in contact with the optics and detector. It is kept under vacuum (10^{-8} – 10^{-9} Torr) by a turbo-molecular pump with a small hydrocarbon mechanical backing pump.

2.4 Detection

The quadrupole mass spectrometer (QMS) is used to characterize our droplet beam by the presence of He_n^+ peaks separated every 4 amu, shown as the blue trace in Fig. 3 below. The impurities or pick-up species can be identified by their respective masses as well. The QMS is capable of performing mass selective measurements where the mass channel can be chosen to eliminate contamination from unwanted ionization products. Electron impact ionization features electrons ~70 eV that impact the helium nanodroplets to form a He^+ ion, leading to further fragmentation of the droplet. When the beam contains only He nanodroplets, the positive charge ends up as a He_n^+ cluster with a mass spectrum identical to the blue spectrum in Fig. 2.3 below. The addition of dopants within the droplet causes the positive charge to quickly find the dopant and

ionize it. Because all molecules have an IP lower than helium, they are rapidly ionized upon electron impact ionization. Two different mass detection schemes exist. The first involves operation of the QMS in “rf-only” mode; where all masses greater than 6 amu are allowed to pass to the detector. The second mode allows us to fix the DC-voltage to a single mass-to-charge ratio to discriminate between possible contamination of the droplet.

The mass spectra of the sequential pick-up of allyl radical + O_2 are shown in Fig. 2.3. This plot shows the evolution of mass signal with an increase in pyrolysis source current (i.e., an increase in temperature). The most notable fragments of the ionized precursor molecule are m/z=27 $(C_2H_3)^+$, 29 $(C_2H_5)^+$, 30 $(CH_2O)^+/(NO)^+$, 39 $(C_3H_3)^+$, and 41 u $(C_3H_5)^+$.[4] Figure 2.3d shows the mass spectrum as O_2 is added downstream while the pyrolysis source current remains constant at 3.0 amps (~800 K). By comparing (c) to (d), an obvious change is the appearance of mass 32 amu, corresponding to molecular oxygen, but no other changes are relevant.

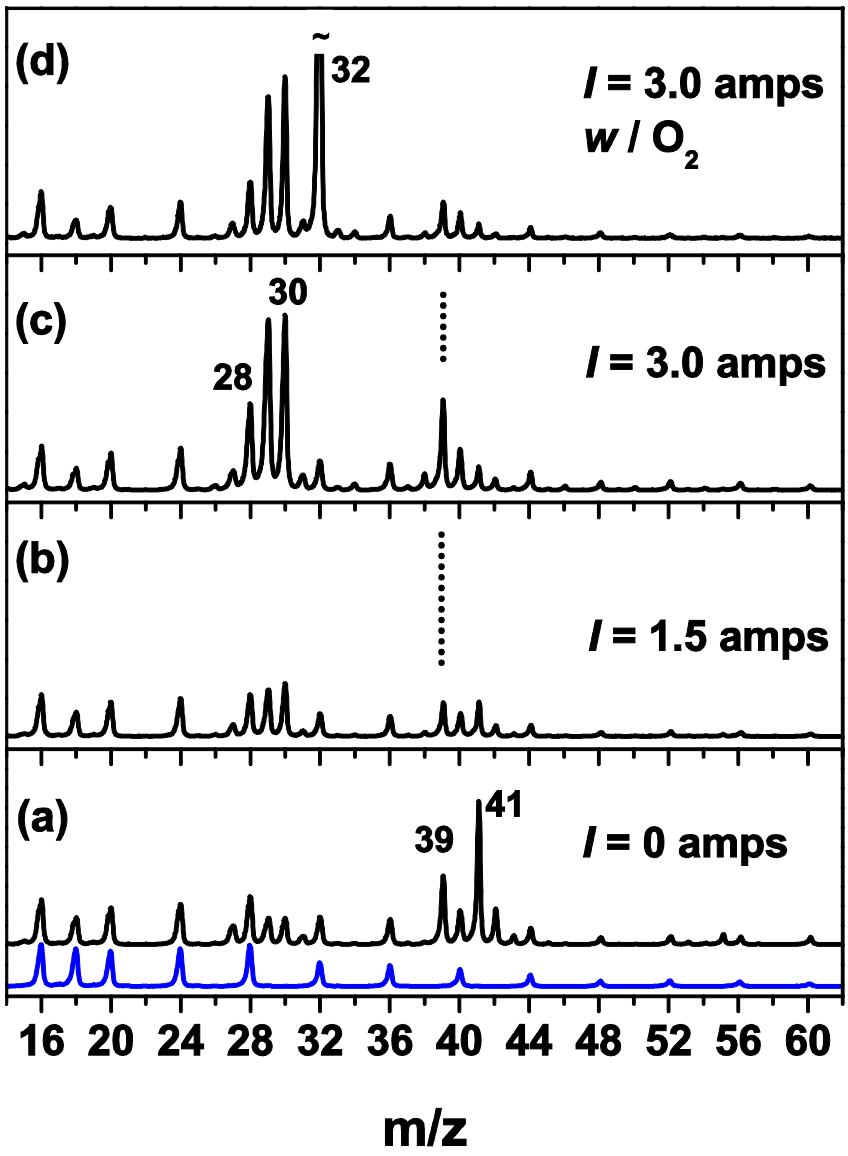

Fig. 2.3. Droplet beam mass spectrum as current increases from 0 to 3 amps, (a) to (c), and with O_2 added in (d).

2.5 Infrared (IR) Spectroscopy

Because the ionization potential (IP) of He is ~24.6 eV, infrared light can pass through the droplet beam freely. When a dopant is added to the droplet beam, the rovibrational motion of the dopant can be excited using an IR laser. The mass spec ion signal is reduced when the beam is depleted. This depletion in signal intensity is due to the evaporation of He atoms and subsequent reduction in the cross sectional area of the

beam. This occurs through the relaxation of vibrationally excited molecules within the droplet that are in resonance with the IR light. The mass spectrum of the allyl radical showed a change in signal at various peaks, but 39 amu was chosen because better spectroscopy signal was obtained using it as compared to other mass channels. The IR spectrum of allyl (a-c) and allyl peroxy (d) is shown below in Fig. 2.4. The * and # indicate allyl + NO/CH_2O and allyl peroxy bands, respectively.

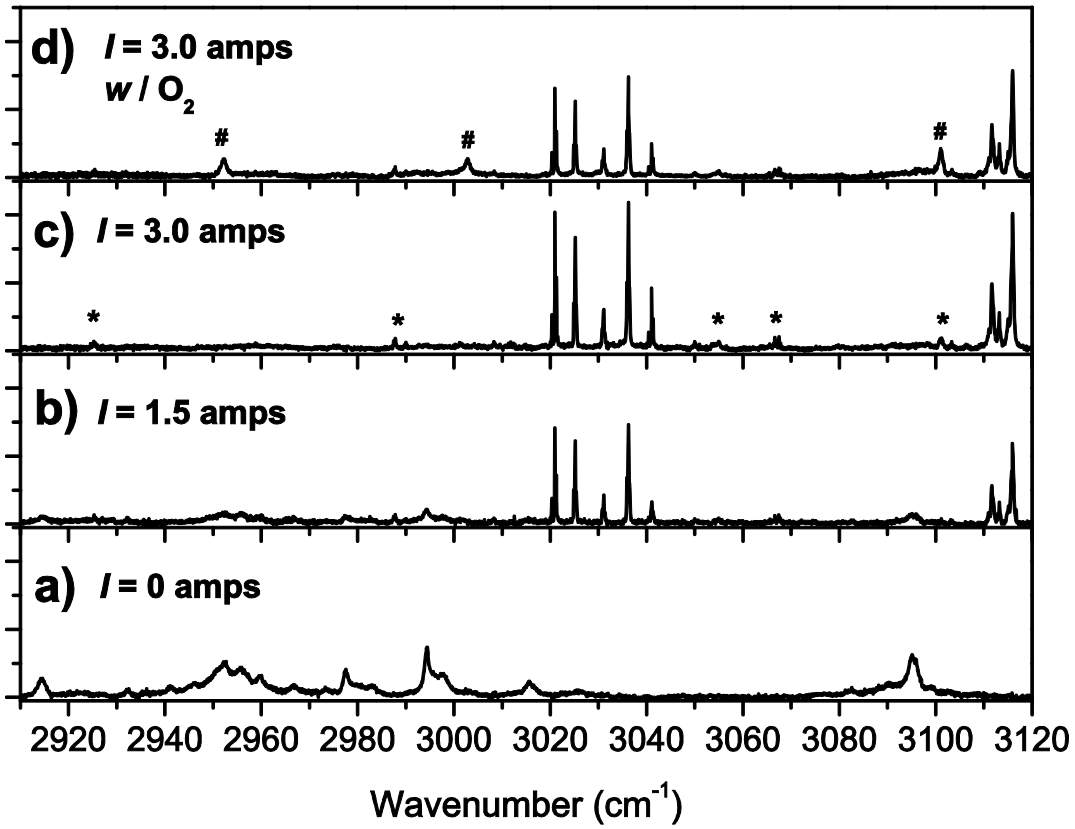

Fig. 2.4. IR spectroscopy signal of allyl radical and allyl peroxy radical from 2900 – 3120 cm^{-1}. The graph shows the evolution with increase in pyrolysis current (a) through (c), as well as the addition of O_2 in (d).

2.6 Description of laser and optical equipment

An Aculight Argos IR cw-OPO (3, in Fig. 2.5 below) is used with a 1064 nm seed laser (1) as the pump, which provides wavelength tuning from 2580-4000 cm^{-1}.[10] The seed laser feeds into a diode-pumped fiber amplifier (2) prior to entering the OPO resonator cavity. The exit of the OPO cavity features three beams: signal, pump, and idler. The signal and pump beams are dumped upon exit (4, 5). The idler beam is then split for three different purposes using CaF_2 beam splitters (6). These purposes include detection via a Power meter (7), Wavemeter (8), and the entrance into a Fabry Perot scanning etalon (9). A Glan Taylor polarizer (10) can be used, if necessary, to separate between s and p-polarized light. As the OPO idler wavelength is tuned, an optical chopper (11), which is typically operated at ~100 Hz, allows the ability for lock-in detection of the laser induced depletion of the ion signal. The gold steering mirrors are designated by Au. The HENDI spectrometer (12) is shown again to illustrate entrance of the laser beam into the spectrometer. The beam that contributes to optical excitation for experiments is the idler beam and enters the spectrometer counter-propagating to the helium droplet beam.

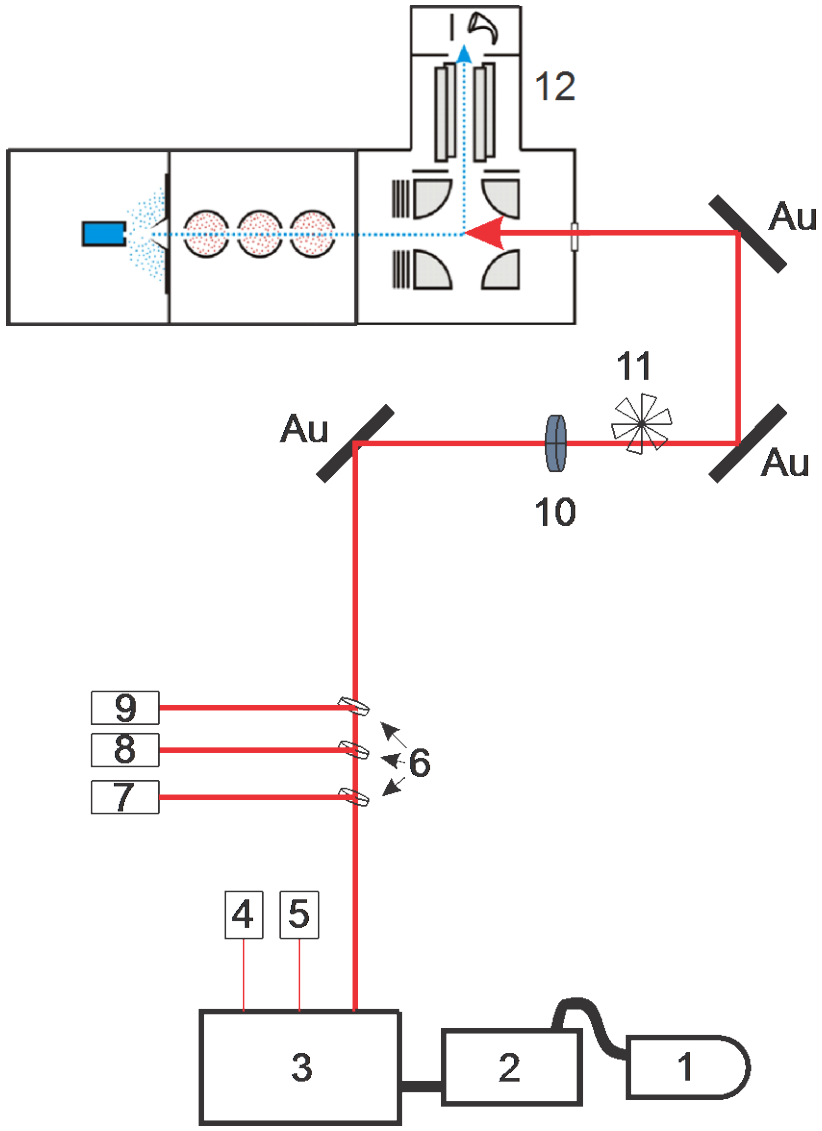

Fig. 2.5. Experimental diagram of the cw-OPO laser system coupled to the HENDI spectrometer.

References

1. Becker, E. W.; Klingelhofer, R.; Lohse, P.; Naturforsch, Z. A 16A, 1259 (1961).
2. Lewerenz, M.; Schilling, B.; Toennies, J. P. *Chem. Phys. Lett.* **1993**, 206, 381-387.
3. E. L. Knuth, B. Schilling, and J. P. Toennies, Proceedings of the 19th International Symposium on Rarefied Gas Dynamics (Oxford University Press, 1995), pp. 270−276.
4. Leavitt, C. M., Moradi, C. P., Acrey, B. W., Douberly, G. E. *J. Chem. Phys*. 2013, 139, 234301.
5. Choi, M. Y.; Douberly, G. E.; Falconer, T. M.; Lewis, W. K.; Lindsay, C. M.; Merritt, J. M.; Stiles, P. L.; Miller, R. E. International Reviews in Physical Chemistry 2006, 25, 15-75.
6. Küpper, J.; Merritt, J. M.; Miller, R. E. *J. Chem. Phys.* 2002, *117*, 647-652.
7. Moradi, C. P.; Morrison, A. M.; Klippenstein, S. J.; Goldsmith, C. F.; Douberly, G. E. *J. Phys. Chem. A* 2013, *117*.
8. Toennies, J. P.; Vilesov, A. F. *Angewandte Chemie-International Edition* 2004, 43, 2622-2648.
9. Toennies, J. P.; Vilesov, A. F. Annual Review of Physical Chemistry 1998, 49, 1-41.
10. Morrison, A. M.; Liang, T.; Douberly, G. E. *Rev. Sci. Instrum.* **2013**, 84, 013102/1–013102/8.

CHAPTER 3

OXYGEN ATOM SOURCE

3.1 Background

Atomic oxygen (AO) sources have been of interest in various fields, but the space and atmospheric chemistry communities have encouraged their development over the last two decades. Beginning in the late 1980's, AO sources were developed using various dissociation approaches. This method of making a supersonic beam of AO involves heating a mixture containing O_2 gas to high enough temperature such that dissociation occurs. These supersonic beam sources are capable of producing AO beams with average kinetic energies in the range of 0.2-5 eV. Typical discharge sources for AO production are RF, [1-3] microwave, [4] and laser sustained discharges.[5] The AO flux of the sources mentioned above vary from 10^{11}-10^{15} atoms cm^{-2} s^{-1}. Other types of AO production methods mentioned above include: laser detonation, [6] ion neutralization, [7] and photodissociation.[8] The major drawback to these AO sources is that they typically contain byproducts in the form of unwanted contamination. Possible contamination products include molecular oxygen, ions, excited species, and UV-light, in addition to the carrier gas. The UV-light is a potential contaminant where light in the UV range is capable of breaking bonds of oxygen containing species: O_2, NO_2, or O_3.

Two different sources that are capable of producing the ground triplet state of atomic oxygen are available, the first of which lead to a joint patent in 1994 by a team of scientists from the University of Florida and NASA.[9-14] They designed a clean,

hyperthermal oxygen atom generator that is capable of producing AO with an average kinetic energy of 5 eV and a flux as high as 10^{13} atoms/cm^2-s.[11, 13] This was the first design to offer a source O (^{3}P), but due to the complex nature of the oxygen atom production method, this source is not ideal for use with our experimental technique.

Another type of AO source utilizes the thermal dissociation of molecular oxygen flowing through a heated iridium capillary tube. This mechanism is similar to that of high temperature pyrolysis. A cracking tube heated by a surrounding filament provides an efficient thermal cracking of O_2 molecules to produce atomic oxygen (AO). This method provides a clean beam. Iridium is used due to low oxidative properties, low vapor pressure (~1.0 x 10^{-6} Torr @ 2000 K), and high melting point (~2680 K). A tungsten filament is coiled around the Ir tube and extends approximately half the length of the tube. A detailed picture of this design, see Fig. 10, shows the materials used in the construction of this device. Thermal isolation and water cooling are required due to the high temperature of dissociation. This type of source is commercially available from MBE-Komponenten, but due to the high cost, we have decided to modify one of our present sources currently being used for pyrolysis.[15-17] The fact that this source represents an atomic oxygen beam with only ground electronic state species is in contrast to alternative production methods available from commercial sources. Commercial sources such as plasma arc tubes are convenient in their design, but higher in cost than having a piece of equipment built. These sources usually have an O atom purity of 40-90 % with the alternate impurities being either O_2 or the carrier gas sustained in the plasma, namely He or Ar. A pure beam of O (^{3}P) does not harbor any unwanted ionized or excited state species.

3.2 Helium Solvation

The solvation of atoms in helium has been studied previously.[18, 19] A fundamental calculation was performed to ensure that an oxygen atom would indeed solvate into the helium droplet. The calculation involved finding an ancilotto parameter, λ, which is a characteristic of the physics of helium-solvation. This method has been used for clusters and other solvating species and was discovered by Ancilotto and co-workers in 1995.[18] The Ancilotto parameter,

$$\lambda = \frac{\rho \epsilon r_{min}}{\sigma 2^{1/6}},$$

is dimensionless and is simply a ratio of the dopant-helium attraction to the energy cost of forming a helium surface upon solvation of an oxygen atom. The constants in the equation above are: $\sigma = 0.179$ cm^{-1}, Å^{-2} = surface tension of liquid He, and $\rho = 0.0218$ Å^{-3} = density of liquid helium. The two variables that the ancilotto parameter depends on are equilibrium well depth, ε, and equilibrium bond distance, r_{min} associated with the O (^{3}P)-He pair potential. Douberly and Miller estimate that an Ancilotto parameter greater than 1.9 is needed for solvation within the helium droplet.[19] Upon performing the calculation at the CCSD(T)/aug-cc-pVQZ level of theory ($r_{min} = 3.0228$ Å, $\varepsilon = 22.99$ cm^{-1}), we found that an O (^{3}P) atom would become solvated within the droplet because of the large Ancilotto parameter, which is approximately 7.5.

3.3 Oxygen Atom Source

The modification of a source similar to the one pictured in Figure 3.1 has been proposed and features the same water cooled copper electrodes (orange). The major differences are in the materials used to make the source. The highly reactive nature of O (^{3}P) atoms necessitates the use of materials that won't degrade due to their exposure to

atomic oxygen.

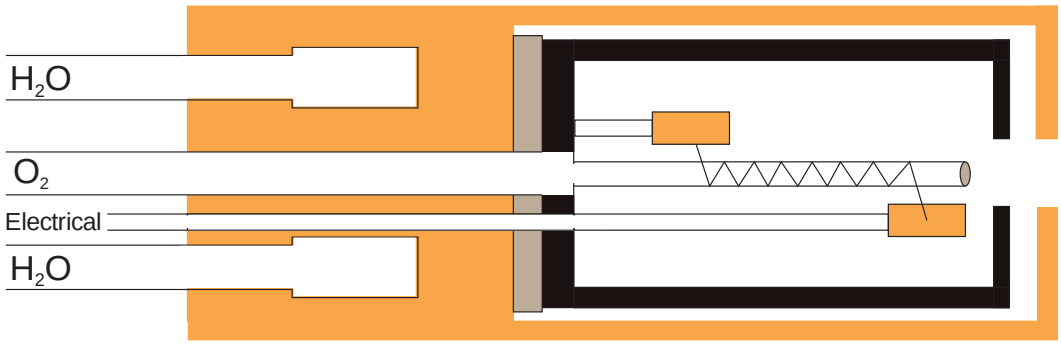

Fig. 3.1. Proposed O atom source design. (Orange = Cu, Black = Ta, Grey = Al_2O_3).

This design features slight modifications from an oxygen beam source that is commercially available from MBE Komponenten.[15-17] The iridium (Ir) cracking tube is heated radiatively by a heated tungsten filament to assure optimum dissociation of molecular oxygen. The capillary tube is operated between 1990 - 2200 K by application of a variable AC voltage applied to the tungsten filament. The dimensions of the Ir tube are optimally 50 mm in length with an inner diameter of 1 mm and an outer diameter of 2 mm. Iridium is difficult to machine and only a few companies in the United States offer iridium tube to the public. Refracto Technologies Corp., located in New York, sells iridium in several different forms. They have the capability to manufacture iridium in tubular form. The quote we received for the length of iridium tube specified above was approximately three thousand dollars. A tantalum heat shield surrounds the emission cavity and provides the best compromise between workability and durability. We expect the O atom production response to be directly related to the input current at the electrode. As we increase the input current, we should see an increase in O atom signal. This design should be capable of an O atom flux in the range of 10^{14}- 10^{16} cm^{-2}-s^{-1}, depending on the conditions.

References

1. Sibener, S. J.; Buss, R. J.; Ng, C. Y.; Lee, Y. T. *Rev. Sci. Instr*. **51**, 167 (1980).
2. Nikiforov, A. P.; Skurat, V. E. *Chem. Phys. Lett*. **212**, 43 (1993).
3. Pollard, J. E. *Rev. Sci. Instr*. **63**, 1771 (1992).
4. Arnold, G. S.; Peplinski, D. R.; Cascarano, F. M. *J. Spacecraft* **24**, 454 (1987).
5. Cross, J. B.; Blais, N. C. *Progress in Astronautics and Aeronautics* **116**, 143 (1989).
6. Caledonia, G. E.; Krech, R. H.; Green, B. D. *AIAA J.* **25**, 59 (1987).
7. Orient, O. J.; Chutjian, A.; Murad, E. *Phys. Rev*. **A41**, 4106 (1990).
8. Kinugawa, Y.; Sato, T.; Arikawa, T. *J. Chem. Phys*. **93**, 3289 (1990).
9. Outlaw, R. A.; Hoflund, G. B.; Corallo, G. R. Appl. Surf. Sci. **1987**, 28, 235.
10. Hoflund, G. B.; Davidson, M. R.; Outlaw, R. A. Surf. Interface Anal. **1992**, 19, 325.
11. Outlaw, R. A.; Davidson, M. R. J. Vac. Sci. Technol. A. **1994**, 12, 854- 860.
12. Outlaw, R. A.; Davidson, M. R. Small UHV Compatible Hyperthermal Oxygen Atom Generator. U.S. Patent 5,367,161, Nov. 22, 1994.
13. Shively J., Miglionico C., Roybal R., King T., Robertson R., Baird J., Davis S., and Stein C., "Combined Effects of the Lower Earth Orbit Environment on polymeric materials", *High temperature and environmental effects on polymeric composites*, Vol.2, ASTM STP1302, American Society for Testing and Materials, 1997, pp.223-242.
14. Hoflund, G. B.; Weaver, J. F. *Meas. Sci. Technol*. **5** (1994) 201-204.
15. Tscherisch, K. G.; Bonin,V. *J. Appl. Phys.* **1998**, 84, 4065.

16. Tscherisch, K. G. *J. Appl. Phys.* **2000**, 87, 2565.

17. Eberl, K. MBE-Komponenten. http://www.mbe-komponenten.de/products/mbe-components/gas-sources/obs.php (11/01/2013), Oxygen Atom Beam Source OBS data sheet, MBE-components.

18. Ancilotto, F.; Lerner, P. B.; Cole, M. W. J. Low Temp. Phys. **1995**, 101, 1123-1146.

19. Douberly, G. E.; Miller, R. E. *J. Phys. Chem. A.* **2007**, 111, 7292-7302.

CHAPTER 4

$O\ (^3P) + C_2H_2/C_2H_4/\cdot CH_3$

4.1 Background

Atomic oxygen (AO) is the third most abundant element in the universe, behind hydrogen and helium, respectively.[1] A detailed study of atomic oxygen chemistry is essential for a thorough understanding of atmospheric processes. The fundamental reactions that lead to atomic oxygen in our upper atmosphere (thermosphere) involve photochemical dissociation of molecular oxygen,

$$O_2 + h\nu\ (\lambda < 125\ nm) \rightarrow O\ (^1D) + O\ (^1D)$$
$$O_2 + h\nu\ (125\ nm < \lambda < 260\ nm) \rightarrow O\ (^1D) + O\ (^3P)$$
$$O_2 + h\nu\ (\lambda > 260\ nm) \rightarrow O\ (^3P) + O\ (^3P)\ .[2]$$

The concentration of AO has been simulated with the aid of atmospheric modeling of our thermosphere to yield a concentration of $4.5 \times 10^{11}\ cm^{-3}$ at an altitude of 100 km where the concentrations of molecular and atomic oxygen are approximately equivalent.[3] The concentration of $O\ (^3P)$ is more abundant than O_2 in our upper thermosphere (altitude > 120 km) due to the presence of high-energy ultraviolet radiation ($\lambda < 260$ nm) in this region. The other prominent source of AO in the atmosphere is the photochemical dissociation of ozone (O_3) occurring in the stratosphere, 10-50 km, where the concentration of $O\ (^3P)$ is approximately $10^8 - 10^9\ cm^{-3}$.[4]

$$O_3 + h\nu\ (\lambda < 1180\ nm) \rightarrow O\ (^3P) + O_2$$
$$O_3 + h\nu\ (\lambda < 320\ nm) \rightarrow O\ (^1D) + O_2$$

The collision of excited O (^{1}D) with molecules leads to the stabilization of neutral ground state O (^{3}P). As a reactant in the rate-determining step, O (^{3}P) reacts with ozone which yields two oxygen molecules.[5] There are a number of other multi-step reactions that occur between AO and atmospheric constituents, for example, $O + NO_2 \rightarrow NO + O_2$. The products of this reaction may go on to produce ozone and AO through subsequent reactions. The reactions of NO_x are significant in the destruction of ozone in our atmosphere.[5]

Combustion reactions involving O_2 produce atomic oxygen as an unwanted scavenger. Reactions of ground state neutral AO with unsaturated hydrocarbons are a fundamental chemical process in combustion environments. For example, reaction with O (^{3}P) is believed to be the primary loss mechanism for acetylene (C_2H_2) in flames.[6] Ethylene (C_2H_4) is also present in combustion reactions and along with acetylene is a byproduct of the breakdown of larger hydrocarbons. A common example of this combustion process is revealed in the gasoline combustion engine, where both ethylene and acetylene are detected in the atmosphere as a result.[7] Prior studies of reactions between neutral atomic oxygen and C_2H_2/C_2H_4 include both experimental work[8-10] and theoretical calculations.[11-14] In particular, the O (^{3}P) ground electronic state of oxygen, has been reacted with acetylene and ethylene using Crossed Molecular Beams (CMBs).[8-10] Spectroscopic detection of the products and intermediates associated with these reactions is lacking in both the gas phase and in matrix isolation. The final proposed experiment involves the reaction of O (^{3}P) + methyl radical. The goal will be to isolate the addition intermediate, methoxy radial, *in situ* and attempt to solve the challenging spectroscopic problem that arises due to various angular-momentum couplings within this

molecular radical.

The HENDI technique[15-16], outlined in Chapters 1 and 2 of this thesis, offers us the possibility of studying the hard to trap bound states of combustion intermediates that are difficult to produce with other methods. The design of an AO source will be implemented into our experimental technique via a pick-up cell (PUC). Acetylene and ethylene have already been studied in the helium nanodroplet environment.[17-18] We will probe the relative shifts in the spectra due to presence of AO as compared to that of the hydrocarbon only spectra within the droplets. The proposed reactions to be studied include O (^{3}P) + C_2H_2/C_2H_4/·CH_3. Helium nanodroplet spectroscopy literature is still lacking the inclusion of the effects of open-shell species like oxygen atoms attached to molecules of interest in combustion and atmospheric science. We propose to pick-up these oxygen atoms sequentially with the hydrocarbon molecule of interest and probe the associated reactions that occur between the cold reactants with IR spectroscopy.

4.2 O (^{3}P) + C_2H_2

We will first probe the Acetylene-O (^{3}P) complex. This complex has relevance for both atmospheric and combustion chemistry, because it has been identified as a key intermediate in automobile combustion. The goal is to identify the CH stretching region, possible rotational profiles of acetylene, and possible shifting of peaks due to the addition of oxygen at this correspondingly low temperature. This complex has been studied theoretically by several groups.[11-14] The most recent theory on this complex by Nguyen and co-workers reports a Potential Energy Surface (PES) calculated using CBS-QCI/APNO and (CCSD(T)/6-311++G-(3df,2p)) levels of theory.[14] Due to the entrance barrier predicted around 3.5-4 kcal/mol we do not expect to see many of the

intermediates along the reaction pathway. We should not have any trouble identifying and characterizing the weakly bound van der Waals (vdW) complex (C_2H_2O) in our droplet, assuming that they will interact within the droplet. We are interested in the formation of the di-radical intermediate (HCCHO) due to ground state O atoms being electrophilic and having the ability to add to carbon-carbon double or triple bonds, however we probably will not see this complex due to the entrance barrier. The excess energy required upon bond formation should be absorbed by the helium bath allowing the vdW complex to be sustained in the droplet. The helium bath is capable of dissipating 5 cm^{-1} of energy per helium atom evaporated. The average size of our helium droplets is approximately 4000 He atoms based on the known statistical distribution of droplet sizes. A rotational profile of the complex would be exciting as well.

4.3 O (^{3}P) + C_2H_4

The reaction between O (^{3}P) and C_2H_4 gives us a chance to look at the smallest alkene molecule. Ethylene is also a key intermediate in the oxidation of methane and of larger hydrocarbons. Theoretical calculations performed most recently by Bowman[10] and Nguyen[19] seem to agree in their assignment of the PES. This complex has also been studied by Schatz where they specifically looked at intersystem crossing effects where the potential energy surfaces were calculated using the unrestricted B3LYP/6-31G(d,p) electronic structure method. They used a simplified version of the quasi-classical trajectory surface hopping method in which transitions between triplet-singlet states were only allowed at points where the two surfaces crossed.[20] This reaction has an entrance barrier of approximately 3 kcal/mol and is similar to acetylene in that respect. Oxygen atoms in their triplet ground electronic state undergo an electrophilic addition onto the

C=C bond that forms adducts that are vibrationally excited bi-radicals corresponding to the spin-conservation rule.[18] We once again expect to probe the weakly bound van der Waals complex. We expect to see small shifts as compared to the spectra of ethylene in helium nanodroplets, and we expect completely different rotationally resolved splittings due to the nature of the molecular complex upon the addition of an oxygen atom. The spectrum of ethylene in the He matrix included all four vibrational bands three *a*-type bands (ν_{11}, $\nu_2+\nu_{12}$, and $2\,\nu_{10}+\nu_{12}$) and the lone *b* type band (ν_9) with only small band origin shifts.[18]

4.4 O (^{3}P) + CH_3·

The methoxy radical, CH_3O·, is a proposed, *stable* intermediate of the reaction between O (^{3}P) and ·CH_3. It is a small hydrocarbon radical that is a key player in atmospheric and combustion environments.[21-25] It is also produced from the photochemical oxidation of hydrocarbons and contributes to the presence of HO_2 radicals in the atmosphere.[26-27] The reaction between O and the methyl radical, ·CH_3, has an enthalpy of formation that is approximately -90 kcal/mol.[28] This reaction does not have an initial barrier like the other two proposed reactions and is more exothermic compared to other alkyl + O_2 reactions.[29-32]

Experimental work on the O (^{3}P) + CH_3 radical reaction has been performed recently using a variety of experimental techniques.[33-44] Prior investigations of the electronic ground state ($\tilde{X}^2E$) include rotationally resolved studies that led to observations of dispersed laser fluorescence[33-36], stimulated emission pumping[37, 38] (SEP), microwave absorption[39, 40] and laser magnetic resonance.[41, 42] The SEP rotational spectra revealed two (ν_3, CO stretch & ν_6, CH_3 rock) out of the six fundamentals of the methoxy radical.

Three of the vibrational modes that correspond to the totally symmetric, A_1, representation are: C-H stretching (ν_1), CH_3 umbrella (ν_2), and C-O stretching (ν_3). While the asymmetric C-H stretching (ν_4), CH_3 scissoring (ν_5), and CH_3 rocking (ν_6) are doubly degenerate *E* symmetry modes. Recent jet-cooled spectroscopy (T_{rot} = 26 K) of methoxy in the C-H stretching region was reported by Curl and co-workers.[43-44] They report four bands in this region, corresponding to two perpendicular bands with (ΔP = +1) and two parallel bands ($\Delta P = 0$).[44] They attributed these bands to the ν_1 and ν_4, where the symmetrical CH stretch (ν_1) is expected to be split into two levels by the spin-orbit (SO) effect. The asymmetrical CH stretch (ν_4) is expected to split into four vibronic modes through the combination of SO and Jahn-Teller (JT) couplings. Their work suggested that the higher frequency region (2900-3000 cm^{-1}) assignments were complicated by strong vibronic couplings between two CH stretching vibrations and the overtone and combination levels. A complete experimental analysis of the C-H stretching region (2800-3000 cm^{-1}) has yet to be completed.

The methoxy radical represents a complicated problem for theory that involves a JT effect, as well as SO coupling.[45-46] It has been well established that the methoxy radical has a doubly degenerate electronic ground state (^2E) in C_{3v} symmetry.[47, 48] The methoxy radical experiences Jahn–Teller (JT) distortions along the *e* vibrational modes, which splits the degeneracy into a ($^2A'$, $^2A''$) pair of states. These states differ in orbital occupancy by a $(2a'')^2(7a')\rightarrow(2a'')(7a')^2$ excitation.[49] A recent theoretical spin-vibronic model was developed by Marenich and Boggs to study electronic and nuclear dynamics in twofold degenerate electron systems.[45, 46] They performed calculations with the simultaneous treatment of spin-orbit coupling, all linear and quadratic Jahn-Teller

interactions including multimode couplings, and anharmonic effects up to the sixth order for the CH–stretching.[45] The JT stabilization energy is approximately 270 cm^{-1}. While the SO splitting ($-A_{SO}\zeta_e$) is equal to 134 cm^{-1}.[50] The electronic angular momentum can be quenched by JT distortions and effectively reduce the spin-orbit splitting. The SO coupling can quench the JT distortions, but has a minor effect due to $E_{JT} > -A_{SO}\zeta_e$. These two effects taken together have a great impact on the spectroscopy of $CH_3O\cdot$ and must be included in a molecular Hamiltonian to define suitably the nuclear and electronic dynamics of the methoxy radical.

The low temperature and dissipative environment of helium droplets will allow a possible reinvestigation of the rovibrational CH stretching region of the methoxy radical. The proposed source of AO will be utilized in combination with a precursor (DTBP) that has been shown previously to fragment via thermal dissociation into two CH_3 radicals and two $(CH_3)_2CO$ molecules.[51] We expect to isolate the methoxy radical due to the reaction between O (^3P) and CH_3 being largely exothermic. The dissipation of the ~90 kcal/mol reaction will lead to the evaporation of approximately 6300 He atoms. We will be able to vary our experimental helium nozzle conditions (i.e., temp. & pressure) to make larger droplets to account for the larger amount of He atom evaporation. If we can make large enough droplets to accommodate the reactants, we should not have any trouble studying the rovibrational spectroscopy of this complex radical.

References

1. Anders, E.; Ehihara, M. *Geochimica et Coscmochimica Acta*. **1982**, 46, 2363-2380.
2. Tonokura, K.; Shafer, N.; Matsumi, Y.; Kawasaki, M. *J. Chem. Phys*. **1991**, 95, 3394.
3. Lin, F. J.; Chance, K. V.; et al. *Journal of Geophysical Research: Atmospheres* **1987**, 92, 4325-4336.
4. Anderson, J. G. *Geophysical Research Letters.* **1975**, 2, 231-234.
5. Brasseur, G. P.; Jacob, D. J. Mathematical Modeling of Atmospheric Chemistry. http://acmg.seas.harvard.edu/publications/education/brasseur_jacob/ch3_brasseurjacob_Jun11.pdf (11/01/2013), Atmospheric Chemical Processes, Chapter 3.
6. Miller, J. A.; Kee, R. J.; Westbrook, C. K. *Annu. Rev. Phys. Chem.* **1990**, 41, 345-387.
7. Whitby, R. A.; Altwicker, E. R. *Atmos. Env*.**1977**, 12, 1289-1296.
8. Schmoltner, A. M.; Chu, P. M.; Lee, Y. T. J. Chem. Phys. **1989**, 91, 5365.
9. Schmoltner, A. M.; Chu, P. M.; Brudzynski, R. J.; Lee, Y. T. *J. Chem. Phys*. **1989**, 91, 6926.
10. Fu, B.; Han, Y. C.; Bowman, J. M.; Leonori, F.; Angelucci, L.; Balucani, N.; Occhiogrosso, A.; Petrucci, R.; Casavecchia, P. J. Chem. Phys. **2012**, 137, 22A532.
11. Harding, L. B. *J. Phys. Chem*. **1981**, 85, 10-11.
12. Harding, L. B.; Wagner, A. F. *J. Phys. Chem*. **1986**, 90, 2974-2986.
13. Huang, X.; Xing, G.; Bersohn, R. J. Chem. Phys. **1994**, 101, 5818.

14. Nguyen, T. L.; Vereecken, L.; Peeters, J. J. Phys. Chem. A. **2006**, 110, 6696-6706.

15. Toennies, J. P.; Vilesov, A. F. Superfluid Helium Droplets: A Uniquely Cold Nanomatrix for Molecules and Molecular Complexes. Angew. Chem., Int. Ed. **2004**, 43, 2622−2648.

16. Choi, M. Y.; Douberly, G. E.; Falconer, T. M.; Lewis, W. K.; Lindsay, C. M.; Merritt, J. M.; Stiles, P. L.; Miller, R. E. Infrared Spectroscopy of Helium Nanodroplets: Novel Methods for Physics and Chemistry. Int. Rev. Phys. Chem. **2006**, 25, 15−75.

17. Nauta, K.; Miller, R. E. *J. Chem. Phys*. **115**, 8384 (2001).

18. Lindsay, C. M.; Miller, R. E. *J. Chem. Phys*. **2005**, 122, 104306/1−104306/9.

19. Nguyen, T. L.; Vereecken, L.; Hou, X. J.; Nguyen, M. T.; Peeters, J. J. Phys. Chem. A. **2005**, 109, 7489-7499.

20. Hu, W.; Lendvay, G.; Maiti, B. Schatz, G. C. *J. Phys. Chem. A.* **2008**, 112, 2093-2103.

21. Westbrook, C. K.; Dryer, F. L. *Prog. Energy Combust. Sci.* **10**, 1 (1984).

22. Williams, B. A.; Flemming, J. W. *Chem. Phys. Lett.* **221**, 27 (1994).

23. Zabarnick, S. Combust. Flame **85**, 27 (1991).

24. Finlayson, B. J.; Pitts, J. N. *Atmospheric Chemistry* (Wiley, New York, 1986).

25. Hendry, D. G. *J. Phys. Chem.* **81**, 2483 (1977).

26. Aikin, A. C. *J. Geophys. Res.* **87,** 3105 (1982).

27. Perner, D.; Platt, U.; Trainer, M. et al. *J. Atmos. Chem.* **5**, 185 (1987).

28. Marcy, T. P.; Diaz, R. R.; Heard, D.; Leone, S. R.; Harding, L. B.; Klippenstein,

S. J. *J. Phys. Chem. A* **105**, 8361-8369 (2001).

29. Uy, D.; Davis, S.; Nesbitt, D. J. *J. Chem. Phys.* **1998**, *109*, 7793-7802.

30. Han, J. X.; Utkin, Y. G.; Chen, H. B.; Hunt, N. T.; Curl, R. F. *J. Chem. Phys.* **2002**, *116*, 6505-6512.

31. Nandi, S.; Arnold, P. A.; Carpenter, B. K.; Nimlos, M. R.; Dayton, D. C.; Ellison, G. B. *J. Phys. Chem. A* **2001**, *105*, 7514-7524.

32. Leavitt, C. M.; Moradi, C. P.; Acrey, B. W.; Douberly, G. E. *J. Chem. Phys.* **139**, 234301 (2013).

33. Foster, S. C.; Misra, P.; Lin, T.; Damo, C. P.; Carter, C. C.; Miller, T. A. *J. Phys. Chem.* **92**, 5914 (1988).

34. Liu, X.; Damo, C. P.; Lin, T.-Y. D.; Foster, S. C.; Misra, P.; Yu, L.; Miller, T. A. *J. Phys. Chem*. **93**, 2266 (1989).

35. Inoue, G.; Akimoto, H.; Okuda, M. *Chem. Phys. Lett.* **63**, 213 (1979).

36. Lee, Y. Y.; Wann, G.-H.; Lee, Y.-P. *J. Chem. Phys.* **99**, 9465 (1993).

37. Geers, A.; Kappert, J.; Temps, F.; Sears, T. J. *J. Chem. Phys.* **98**, 4297 (1993).

38. Temps, F. *Adv. Ser. Phys. Chem.* **4**, 375 (1995).

39. Y. Endo, S. Saito, and E. Hirota, *J. Chem. Phys.* **81**, 122 (1984).

40. Momose, T.; Endo, Y.; Hirota, E.; Shida, T. *J. Chem. Phys*. **88**, 5338 (1988).

41. Russell, D. K.; Radford, H. E. *J. Chem. Phys.* **72**, 2750 (1980).

42. Radford, H. E.; Russell, D. K. *J. Chem. Phys.* **66**, 2222 (1977).

43. Han, J.; Utkin, Y.; Chen, H.; Burns, L. A.; Curl, R. F. *J. Chem. Phys.* **117**, 8 (2002).

44. Han, J.; Hu, S.; Chen, H.; Utkin, Y.; Brown, J. M.; Curl, R. F. *Phys. Chem. Chem. Phys*., **2007**, 9, 3725–3734.

45. Marenich, A. V.; Boggs, J. E. *J. Chem. Phys.* **122**, 024308 (2005).

46. Marenich, A. V.; Boggs, J. E. *Chem. Phys. Lett*. **404**, 351–355 (2005).

47. Brossard, S. D.; Carrick, P. G.; Chappell, E. L.; Hulegaard, S. C.; Engelking, P. C. *J. Chem. Phys.* **84**, 2459 (1986).

48. Barckholtz, T. A.; Miller, T. A. *Int. Rev. Phys. Chem.* **17**, 435 (1998).

49. Petraco, N. D. K.; Allen, W. D.; Schaefer, H. F. *J. Chem. Phys.* **116**, 10229-10237 (2002).

50. Marenich, A. V.; Boggs, J. E. *J. Mol. Struct.*, **780–81**, 163–170 (2006).

51. Morrison, A. M.; Agarwal, J.; Schaefer, H. F.; Douberly, G. E. *J. Phys. Chem. A.* **2012**, 116, 5299-5304.

CHAPTER 5

CONCLUSION

The HENDI technique, outlined in Chapters 1 and 2, offers the possibility of studying hard to trap bound states of combustion intermediates that are difficult to produce with other methods. The design of an AO source, discussed in Chap. 3, will be implemented into our experimental technique via a pick-up cell (PUC). This AO source design involves slight modifications to our current pyrolysis source. Helium nanodroplet spectroscopy literature is still lacking the inclusion of the effects of open-shell species like oxygen atoms attached to molecules of interest in combustion and atmospheric science. We proposed to pick-up these oxygen atoms sequentially with the hydrocarbon molecule of interest and probe the associated reactions that occur between the cold reactants with IR spectroscopy.

The Acetylene-O (^{3}P) and Ethylene- O (^{3}P) complexes were proposed in Chapter 4. The goal is to identify the CH stretching region, possible rotational profiles of acetylene, and possible shifting of peaks due to the addition of oxygen at this correspondingly low temperature. Acetylene and ethylene have already been studied in the helium nanodroplet environment.[1, 2] Possible shifts in the spectra due to presence of AO were discussed as compared to that of the hydrocarbon only spectra. Ethylene (C_2H_4) is also present in combustion reactions and along with acetylene is a byproduct of the breakdown of larger hydrocarbons. Entrance barriers, approximately 3 kcal/mol, are predicted by theoretical calculations for these two reactions.[3-9] Due to these barriers, we

do not expect to see many of the intermediates along the reaction pathway. We should not have any trouble identifying and characterizing the weakly bound van der Waals (vdW) complexes (C_2H_2O & C_2H_4O) in our droplet, assuming that they will interact within the droplet.

The final proposed reaction is O (^3P) + methyl radical. The methoxy radical, $CH_3O\cdot$, is a proposed, *stable* intermediate of this reaction. The reaction between O (^3P) and the methyl radical, $\cdot CH_3$, has an enthalpy of formation that is approximately -90 kcal/mol.[10] This reaction does not have an initial barrier like the other two proposed reactions. The methoxy radical represents a complicated problem for theory that involves a JT effect, as well as SO coupling.[11, 12] The electronic angular momentum can be quenched by JT distortions and effectively reduce the spin-orbit splitting.

The low temperature and dissipative environment of helium droplets will allow a possible reinvestigation of the ro-vibrational CH stretching region of the methoxy radical. The proposed source of AO will be utilized in combination with a precursor (DTBP) that has been shown previously to fragment via thermal dissociation into two CH_3 radicals and two $(CH_3)_2CO$ molecules.[13] We expect to isolate the methoxy radical due to the reaction between O (^3P) and CH_3 being largely exothermic. We will be able to vary our experimental helium nozzle conditions (i.e., temp. & pressure) to make larger droplets to account for the larger amount of He atom evaporation.

References

1. Nauta, K.; Miller, R. E. *J. Chem. Phys*. **115**, 8384 (2001).
2. Lindsay, C. M.; Miller, R. E. *J. Chem. Phys*. **2005**, 122, 104306/1−104306/9.
3. Fu, B.; Han, Y. C.; Bowman, J. M.; Leonori, F.; Angelucci, L.; Balucani, N.; Occhiogrosso, A.; Petrucci, R.; Casavecchia, P. J. Chem. Phys. **2012**, 137, 22A532.
4. Harding, L. B. *J. Phys. Chem*. **1981**, 85, 10-11.
5. Harding, L. B.; Wagner, A. F. *J. Phys. Chem*. **1986**, 90, 2974-2986.
6. Huang, X.; Xing, G.; Bersohn, R. J. Chem. Phys. **1994**, 101, 5818.
7. Nguyen, T. L.; Vereecken, L.; Peeters, J. J. Phys. Chem. A. **2006**, 110, 6696-6706.
8. Nguyen, T. L.; Vereecken, L.; Hou, X. J.; Nguyen, M. T.; Peeters, J. J. Phys. Chem. A. **2005**, 109, 7489-7499.
9. Hu, W.; Lendvay, G.; Maiti, B. Schatz, G. C. *J. Phys. Chem. A.* **2008**, 112, 2093-2103.
10. Marcy, T. P.; Diaz, R. R.; Heard, D.; Leone, S. R.; Harding, L. B.; Klippenstein, S. J. *J. Phys. Chem. A* **105**, 8361-8369 (2001).
11. Marenich, A. V.; Boggs, J. E. *J. Chem. Phys.* **122**, 024308 (2005).
12. Marenich, A. V.; Boggs, J. E. *Chem. Phys. Lett*. **404**, 351–355 (2005).
13. Morrison, A. M.; Agarwal, J.; Schaefer, H. F.; Douberly, G. E. *J. Phys. Chem. A.* **2012**, 116, 5299-5304.